Gas Phase Hydrotreatment of Chlorophenols over Pd Catalysts as an Alternative Route to Cyclohexanone

Gas Phase Hydrotreatment of Chlorophenols over Pd Catalysts as an Alternative Route to Cyclohexanone

Santiago Gómez-Quero[†],

Fernando Cárdenas-Lizana and Mark A. Keane[*]

Chemical Engineering, School of Engineering and Physical Sciences,

Heriot-Watt University, Edinburgh EH14 4AS, Scotland

[†]Present address: Avantium, Zekeringstraat 29, Amsterdam 1014 BV, The Netherlands

***corresponding author: tel.: +44(0)131 4514719, e-mail: M.A.Keane@hw.ac.uk**

Abstract

We have established viability of cyclohexanone (C6ONE) production *via* coupled gas phase (1 atm, 423 K) continuous hydrodechlorination/hydrogenation of mono- and di-chlorophenols over bulk Pd and Pd/Al_2O_3. The catalysts have been characterised by temperature programmed reduction, H_2 chemisorption, powder XRD and TEM analyses. Hydrodechlorination is not a thermodynamically limiting step where under catalytic control we achieve significantly greater C6ONE yields relative to those from standard phenol hydrogenation. We account for this response in terms of a direct chlorophenol → C6ONE conversion facilitated by electron delocalisation in the intermediate generated *via* electrophilic hydrogen cleavage of C–Cl bond(s). The C6ONE selectivity/conversion profiles coincided for bulk and supported Pd and we demonstrate structure sensitivity for the production of C6ONE from 2,4-dichlorophenol with higher specific rates over larger Pd particles (2→250 nm).

Key words: Cyclohexanone; chlorophenol(s); Pd catalysts; coupled hydrodechlorination/hydrogenation.

1. Introduction

Cyclohexanone (C6ONE) is commercially important in the production of nylon (C6ONE → caprolactam → nylon 6; C6ONE → adipic acid → nylon 6,6), as a solvent (in lacquers and varnishes) and as a stabiliser/homogeniser (in soaps and detergents) [1,2]. Industrial C6ONE production involves: (a) oxidation of cyclohexane over Co in the liquid phase (T = 413-453 K; P = 8-20 atm) [3]; (b) dehydrogenation of cyclohexanol (C6OH) over Cr-Cu oxides, Ni, ZnS or Zn-Fe (T = 673-723 K; P = 1 atm) [4,5]; (c) hydrogenation of phenol (PhOH) over supported Pd, Pt, Ir or Ru (T = 413-443 K; P = 1 atm) [6]. Each of these routes presents drawbacks. Cyclohexane oxidation generates low C6ONE yields (Y_{C6ONE} = 3–4%) [7,8] and the feedstock is flammable under reaction conditions [9]. C6OH dehydrogenation is endothermic necessitating high temperatures (523-573 K) to achieve appreciable C6ONE production where PhOH [4] and cyclohexene [5] are significant by-products (up to 80% selectivity). In gas phase PhOH hydrogenation the equilibrium conversion falls below 80% at $T \geq$ 530 K [10] and higher catalytic conversion is hampered by temperature-induced desorption of PhOH at $T \geq$ 433 K [11]. Nevertheless, this is the preferred route where Pd-based catalysts exhibit the best performance although, as noted in a recent review [6], high cyclohexanone selectivity (>95%) at elevated phenol conversion (>80%) remains a challenge. Selectivity to the ketone over Pd has been linked to the *d*-character of the metal [11] as the complete *d* shell ([Kr] $4d^{10}$) promotes shielding of valence 5*s* electrons [12] that enhances hydrogenation of PhOH to C6ONE (*via* tautomerisation of the 1-cyclohexenol intermediate, see Fig. 1) [13]. The C6ONE purity from phenol is low for industrial applications, necessitating down-stream purification steps in the form of at least three vacuum distillation columns [14].

Chlorophenols are widely available in the industry pool as intermediates in the manufacture of agricultural chemicals, pharmaceuticals and dyes [15] and represent readily available starting material (*e.g.* concentration of chlorophenol in industrial sewage = 0.1-10 mg/L [16]). Recent literature on batch hydrotreatment of chlorophenol(s) has focused on environmental remediation in terms of controlled chlorine removal [17]. C6ONE has been identified as a product in the catalytic hydrodechlorination/hydrogenation of chlorophenols [18,19] although reported studies have established low yields to C6ONE ($Y_{C6ONE} \leq$ 35%) [20-22]. This transformation involves consecutive/parallel steps shown in Fig. 1. Baumgarten *et al.* [23] studying the hydroprocessing of 2-chlorophenol (2-CP) over polymer supported Pt correlated C6ONE content in the product stream with a reduction in Pt electron density due to support effects. Roy and co-workers [24] recorded exclusive formation of C6OH using $NaBH_4$ as hydrogen donor in the reaction of 2,6-dichlorophenol (2,6-DCP) over Pd/Al_2O_3 while the formation of C6ONE was favoured with H_2 (4 atm) as reducing agent. The multiple

advantages (*e.g.* increased reproducibility, scalability, safety and energy efficiency) of continuous methods for small and large scale chemical production has been the subject of several recent reviews and a move from batch to continuous processing has been identified as critical for sustainable production in the chemical industry [25-29]. We report here the first feasibility study directed at continuous gas phase C6ONE production and evaluate the benefits of (mono- (CP) and di- (DCP)) chlorophenol → C6ONE relative to conventional synthesis from PhOH. Palladium has been identified as the most effective metal in catalytic hydrodechlorination [30]. As metal dispersion plays a critical role in catalytic hydrodechlorination [17] and hydrogenation [31], we have investigated the role of Pd particle size and consider the catalytic action of bulk Pd as a benchmark against which to assess the performance of Pd/Al_2O_3.

2. Experimental

2.1. Catalyst preparation and activation

Commercial (1.2% w/w) Pd/Al_2O_3 catalyst was obtained from Sigma-Aldrich. A physical mixture of $PdO+Al_2O_3$ (Sigma-Aldrich) where the Pd content was equivalent to Pd/Al_2O_3 served as a benchmark. The two systems were activated in H_2 (60 cm^3 min^{-1}) to 573 K to ensure reduction to Pd^0 [32,33]. Activation at higher temperatures (>823 K) results in agglomeration with a decrease in metal dispersion [34] and Pd/Al_2O_3 was subjected to a controlled thermal treatment to 1273 K (sample denoted Pd/Al_2O_3-1273) in order to modify metal dispersion. The Pd content was measured by inductively coupled plasma-optical emission spectrometry (ICP-OES, Vista-PRO, Varian Inc.) from the diluted extract in HF. Prior to reaction the catalysts were sieved (ATM fine test sieves) into a batch of 45 μm average particle diameter. Samples for off-line characterisation were cooled to ambient temperature and passivated in 1% v/v O_2/He.

2.2. Catalyst characterisation

Temperature programmed reduction (TPR) and H_2 chemisorption were performed using the commercial CHEM-BET 3000 (Quantachrome Instruments) unit equipped with a thermal conductivity detector (TCD) for continuous monitoring of gas composition and the TPR Win™ software for data acquisition/manipulation. Samples were loaded into a U-shaped (i.d. = 3.76 mm) quartz cell and heated in 17 cm^3 min^{-1} (Brooks mass flow controlled) 5% v/v H_2/N_2 at 10 K min^{-1} to 573-1273 K. The samples were swept with 65 cm^3 min^{-1} N_2 for 1.5 h, cooled to ambient temperature and subjected to H_2 (BOC, 99.99%) pulse (50 μl) titration under conditions (H_2 partial pressure <0.02 atm) that circumvented Pd hydride formation [32]. Pulses were repeated until the signal area was constant (surface saturation) and Pd particle size was estimated on the basis of dissociative chemisorption (Pd/H stoichiometry = 1:1) on spherical metal particles [34]. Hydrogen

chemisorption values were reproducible to within ±5% and values quoted are the mean. XRD analysis was conducted using a Bruker/Siemens D500 incident X-ray diffractometer with Cu Kα radiation. Samples were scanned at 0.02º $step^{-1}$ over the range 20º ≤ 2θ ≤ 90º and diffractograms identified against JCPDS-ICDD standards (Pd (05-0681) and γ-Al_2O_3 (10-0425)). Transmission electron microscopy (TEM) measurements were conducted using a JEOL JEM 2011 TEM unit with a UTW energy-dispersive X-ray detector (Oxford Instruments) operated at an accelerating voltage of 200 kV and employing Gatan DigitalMicrograph 3.4 for data acquisition/manipulation. Samples were dispersed in acetone and deposited on a holey-carbon/Cu grid (300 Mesh). At least 650 individual Pd particles were counted to obtain a surface weighted mean value [35].

2.3. Catalysis procedure

PhOH, 2-CP, 3-CP, 4-CP, 2,3-DCP, 2,4-DCP and 3,4-DCP (≥98%) were supplied by Sigma-Aldrich and used as received. Reactions were carried out in situ at atmospheric pressure following TPR in a fixed bed (10 mm depth) vertical plug-flow glass reactor (i.d. = 15 mm) under operating conditions that minimised heat/mass transport limitations. Reactants were delivered (as aqueous solutions) to the reactor *via* a glass/teflon air-tight syringe and a teflon line using a microprocessor controlled infusion pump (Model 100 kd Scientific) where molar ratio of metal to phenolic flow rate (W/F_{OH}) spanned the range 1×10^{-3} – 1.33 mol_{Pd} h mol_{OH}^{-1} (5-200 mg catalyst). The use of F_{OH} facilitates a direct comparison of process efficiency in terms of Y_{C6ONE} with respect to the "parent" phenolic ring with/without Cl substituent(s). A co-current flow of ultra-pure H_2 (60 cm^3 min^{-1}) was monitored using a Humonics (Model 520) digital flowmeter and maintained at $GHSV = 2 \times 10^4$ h^{-1}. A layer of glass beads above the catalytic bed served as a preheating zone, ensuring that the reactants were vaporised and reached reaction temperature (423 K) before contacting the catalyst. The reaction temperature was continuously monitored by a thermocouple inserted in a thermowell within the catalyst bed. In blank tests, passage of each reactant in a stream of H_2 through the empty reactor or over the support alone, *i.e.* in the absence of Pd, did not result in any detectable conversion. The reactor effluent was frozen in a liquid nitrogen trap for subsequent analysis, which was made using a Perkin-Elmer Auto System XL GC, employing a DB-1 (J&W Scientific) capillary column (i.d. = 0.20 mm, 50 m length, 0.33 μm film thickness). Relative peak area% was converted to mol% using regression equations based on detailed calibration (not shown). A chlorine mass balance was performed by passing the effluent gas through an aqueous NaOH trap (9×10^{-4} mol dm^{-3}, kept under constant agitation at 400 rpm) with independent pH (Hanna HI Programmable Printing pH Bench-Meter) analysis. Repeated reactions with different samples from the same batch of catalyst delivered raw data reproducibility and

carbon mass balance better than ±8%. Taking 2,4-DCP as representative, the overall level of hydrodechlorination (and hydrogenation) is quoted as a fractional conversion ($X_{2,4\text{-}DCP}$):

$$X_{2,4\text{-}DCP} = \frac{C_{2,4\text{-}DCP,0} - C_{2,4\text{-}DCP}}{C_{2,4\text{-}DCP,0}} \quad (1)$$

where $C_{2,4\text{-}DCP,0}$ represents the initial concentration of 2,4-DCP used in the reaction. Fractional selectivity to C6ONE (S_{C6ONE}) is given by

$$S_{C6ONE} = \frac{C_{C6ONE}}{C_{2,4\text{-}DCP,0} - C_{2,4\text{-}DCP}} \quad (2)$$

and the fractional yield (Y_{C6ONE}) calculated from

$$Y_{C6ONE} = X_{2,4\text{-}DCP} \times S_{C6ONE} \quad (3)$$

3. Results and discussion

3.1. Thermodynamic analysis

It is established that gas phase PhOH hydrogenation is thermodynamically restricted [36]. However, we could not find any reported thermodynamic analysis of the combined hydrodechlorination/hydrogenation of chlorophenols. We have evaluated the possibility of thermodynamic limitations by considering consecutive reaction steps (see dashed arrows in Fig. 1) and drawing on reference equilibrium reaction data [36]:

$$K_1 = \frac{\left(P_{PhOH}\right)^2 \left(P_{HCl}\right)^2}{\left(P_{dichlorophenol}\right)\left(P_{H_2}\right)^2} = 89.0 \times \exp\left(\frac{21279}{T}\right) \quad (4)$$

$$K_2 = \frac{P_{C6ONE}}{\left(P_{PhOH}\right)\left(P_{H_2}\right)^2} = \left(2.76 \times 10^{-16}\right) \times \exp\left(\frac{20131}{T}\right) \quad (5)$$

$$K_3 = \frac{P_{C6OH}}{\left(P_{C6ONE}\right)\left(P_{H_2}\right)} = \left(3.68 \times 10^{-7}\right) \times \exp\left(\frac{7897}{T}\right) \quad (6)$$

where K_j represents the equilibrium constant of step j, P_i is the partial pressure of i (total pressure = 1 atm) and T the reaction temperature. Eqn. (4) applies to the full hydrodechlorination of dichlorophenols (to PhOH) while eqns. (5) and (6) represent the partial hydrogenation steps. The conversion (X_i) and equilibrium constants (K_j) at the reaction temperature (423 K) are given in Table 1 where it is evident that all steps are irreversible. Taking into consideration the steps leading to C6ONE formation (X_i = 1) and consumption (X_i = 0.86), the Y_{C6ONE} under conditions of thermodynamic control is 0.14. It must be noted that this yield is the same regardless of the feedstock (chlorophenol(s) or PhOH), *i.e.* the preceding dechlorination steps do not affect equilibrium Y_{C6ONE}.

C6ONE production from chlorophenols is thermodynamically feasible but operation under kinetic/catalytic (rather than thermodynamic) control is required to maximise Y_{C6ONE}.

3.2. Reaction over Pd

3.2.1. Catalyst characterisation

The temperature programmed reduction (TPR) profile for the bulk system is shown in Fig. 2aI and is characterised by a single negative peak (H_2 release) at T_{max} = 386 K. TPR of the Al_2O_3 support (not shown) did not show any detectable H_2 uptake/release over the same temperature range as noted elsewhere [37]. Hydrogen release can be attributed to decomposition of Pd hydride. Room temperature formation of β-Pd hydride is a well-established bulk phenomenon with H_2 migration into the Pd lattice at a partial pressure in excess of 0.02 atm [32]. Hydride composition (H/Pd = 0.69, Table 2) is in good agreement with that reported previously for the bulk metal (0.6–0.7) [38]. Hydrogen titration delivered low uptake (3×10^{-3} mol mol_{Pd}^{-1}, Table 2) with a calculated Pd particle size (d =) of 250 nm. XRD analysis generated the diffractogram pattern shown in Fig. 2bI where reflections at 2θ = 40.1º, 46.7º and 68.1º correspond to the (111), (200) and (220) planes of cubic Pd (JCPDS-ICDD 05-0681, Fig. 2bIV). Palladium particle size from XRD line broadening [35] gave a value (238 nm) in good agreement with H_2 chemisorption.

3.2.2. Catalytic hydrotreatment of (chloro)phenol(s)

Time-on-stream profiles for the hydrotreatment of (mono- and di-) chlorophenols (Fig. 3) show predominant formation (up to 85% mol) of C6ONE. C6OH and PhOH were generated as secondary products with trace quantities (selectivity <2%) of partially dechlorinated products. The temporal variation in product distribution can result from partial catalyst deactivation due to poisoning by HCl (as by-product) and/or coke deposition [39]. Product composition was evaluated from

$$x_i = x_{i,0} \times \exp\left(-\alpha \times \Delta t\right) \tag{7}$$

where x_i represents mole fraction of compound i, Δt the integral time and α is a fitting parameter. Non-linear fitting of the experimental data allows an estimation of initial molar fractions ($x_{i,0}$) and associated initial C6ONE yield ($Y_{C6ONE,0}$) from eqns (1–3); the results are given in Table 3. The $Y_{C6ONE,0}$ values recorded for the hydroprocessing of chlorophenols were appreciably higher than that obtained under thermodynamic equilibrium (0.14). Significantly, $Y_{C6ONE,0}$ from a chlorophenolic feed exceeded that achieved with PhOH. C6ONE production from PhOH occurs *via* formation and tautomerisation of 1-cyclohexenol as intermediate [40] where the equilibrium is thermodynamically shifted in favour of the ketone by 75 kJ mol^{-1} [41]. In the case of

chlorophenols, C6ONE production can proceed through stepwise and/or concerted routes (Fig. 1). If the hydrotreatment of chlorophenols proceeded in a strictly stepwise manner (consecutive hydrodechlorination, hydrogenation and tautomerisation steps) Y_{C6ONE} should not exceed that obtained from PhOH. An alternative route to C6ONE from chlorophenols can involve (electrophilic) attack of the chloroarene by hydrogen to generate a cationic reaction intermediate that is stabilised by electron delocalisation within the aromatic ring [42]. The lone pair of electrons on the hydroxyl substituent serves to stabilise an intermediate bearing the C=O group [43,44] leading to preferential C6ONE formation. The tabulated results support our contention that catalytic conversion of chlorophenols is a feasible alternative for C6ONE production. $Y_{C6ONE,0}$ increased with increasing Cl substitution following the order; PhOH < 2-CP, 3-CP, 4-CP < 2,3-DCP, 2,4-DCP. The response for 3,4-DCP deviates from the general trend (*i.e.* lower $Y_{C6ONE,0}$ and higher $S_{PhOH,0}$), a result suggesting that the relative position of Cl substituents on the ring can influence reaction pathway. An explicit assessment of Y_{C6ONE} dependence on the chlorophenol isomer requires reaction conditions where hydrodechlorination is not complete. This was achieved by lowering the contact time and the resultant C6ONE yields are presented in Fig. 4. Hydrotreatment of dichlorophenols generated consistently higher $Y_{C6ONE,0}$ relative to the monochlorophenol reactants. This can be ascribed to the greater effect of *delocalisation* in the dichlorophenol feed that results in an increased number of favourable resonance forms bearing the C=O group which determines reactivity [17]. Taking the three monochlorophenols, the lowest $Y_{C6ONE,0}$ for the 2-CP feed is consistent with reports in the literature on the hydrotreatment of cresols over a chitosan Pd-complex (SiO_2-CS-Pd) [45] and can be ascribed to *steric* effects [46], *i.e.* similar $S_{C6ONE,0}$ for the three isomers (see Table 3) but lower conversion of 2-CP due to steric hindrance in adsorption/activation [47]. Given the highest $Y_{C6ONE,0}$ achieved with the 2,4-DCP feed (Table 3 and Fig. 4), we chose this as the model reactant to assess the effect of metal particle size on catalytic performance.

3.3. Effect of Pd particle size in the hydrotreatment of 2,4-DCP: reaction over Pd and Pd/Al_2O_3

3.3.1. Catalyst characterisation

Metal dispersion was modified by controlled thermal sintering (see Experimental section and Table 2) of Pd/Al_2O_3. The TPR response for Pd/Al_2O_3-1273 (Profile II) and Pd/Al_2O_3 (Profile III) in Fig. 2a show a single negative peak due to Pd hydride decomposition. Both supported catalysts exhibited lower hydride decomposition temperatures and hydrogen content relative to Pd, which can be ascribed to smaller Pd particle size [32]. Hydrogen chemisorption on Pd/Al_2O_3-1273 (see Table 2) was significantly lower than that recorded for Pd/Al_2O_3 but appreciably greater than Pd. The associated Pd particle size (*d*) decreased in the order Pd (250

nm) > Pd/Al_2O_3-1273 (13 nm) > Pd/Al_2O_3 (2 nm). The XRD profiles (Fig. 2b) reveal reflections at 2θ = 45.8º and 66.8º corresponding to the (400) and (440) planes of cubic γ-Al_2O_3 (JCPDS-ICDD 10-0425, Profile V). A weak signal due to metallic Pd was in evidence for Pd/Al_2O_3-1273 (Profile II) whereas the absence of this XRD signal in Pd/Al_2O_3 (Profile III) suggests the presence of small Pd ensembles. Representative TEM images and associated particle size distributions are shown in Fig. 5 where differences in metal crystal size are in evidence. Pd/Al_2O_3-1273 is characterised by a broader size distribution of nano-scale Pd particles in the range 1-15 nm relative to Pd/Al_2O_3, which presents a more homogeneous distribution of particles in the 1-6 nm size range. The surface area weighted mean Pd particle size (10 nm (Pd/Al_2O_3-1273) and 3 nm (Pd/Al_2O_3)) from TEM analysis agree with the values obtained from H_2 chemisorption.

3.3.2. Catalytic performance in the hydrotreatment of 2,4-DCP

$Y_{C6ONE,0}$ as a function of contact time over all the systems is presented in Fig. 6a where the yield under thermodynamic equilibrium (=0.14) is given by the dotted line. The three catalytic systems showed a decrease in $Y_{C6ONE,0}$ at lower contact times. A direct comparison in terms of $Y_{C6ONE,0}$ at a fixed (W/F_{OH}) is not possible as the profiles do not overlap. In order to facilitate an explicit assessment of structure sensitivity, it is necessary to compare the specific reaction rates (normalised per m^2_{Pd}) for the three catalysts. Initial C6ONE production rate $(R_{C6ONE})_0$ was calculated from the mass balance for a plug flow reactor

$$(R_{C6ONE})_0 = \frac{dF_{C6ONE}}{dW} = \frac{d\left(Y_{C6ONE,0}\right)}{d\left(W/F_{OH}\right)} \tag{8}$$

and the specific rate $(R'_{C6ONE})_0$ estimated from

$$(R'_{C6ONE})_0 = \frac{(R_{C6ONE})_0}{S_{Pd}} \tag{9}$$

where S_{Pd} is the metal surface area (see Table 2). Specific rates increased in the order: Pd/Al_2O_3 (49 × 10^{-4} mol_{C6ONE} h^{-1} m_{Pd}^{-2}) < Pd/Al_2O_3-1273 (68 × 10^{-4} mol_{C6ONE} h^{-1} m_{Pd}^{-2}) < Pd (94 × 10^{-4} mol_{C6ONE} h^{-1} m_{Pd}^{-2}). These results suggest greater intrinsic efficiency for larger Pd particles. A direct comparison of our results with the literature is difficult as the observed structure sensitivity applies to coupled hydrodechlorination/hydrogenation and work to date has considered individual hydrogenation or hydrodechlorination processes in isolation. Our observations find agreement with reported work where increased activity over larger metal particles has been demonstrated for the gas phase hydrodechlorination of chlorophenols [17]. Moreover, higher hydrodechlorination activity has been reported for bulk Ni and Pd when compared with Al_2O_3 supported systems [48]. In the case of PhOH hydrogenation, structure insensitivity has been proposed for supported Pd

[49] but we should highlight the work of Chary *et al.* [50] who recorded higher PhOH turnover frequencies (from < 0.01 s^{-1} to 0.52 s^{-1}) over larger Pd particles (2–8 nm) supported on carbon. The impact of Pd size on the reaction network was assessed from a consideration of the dependence of initial C6ONE selectivity ($S_{C6ONE,0}$) on 2,4-DCP conversion ($X_{2,4\text{-}DCP,0}$) and the results are presented in Fig. 6b. $S_{C6ONE,0}$ increased abruptly at $X_{2,4\text{-}DCP,0} \geq$ 0.8, *i.e.* at high levels of HDC. The trend coincided for the three catalytic systems, indicating insensitivity of the reaction pathway with respect to Pd size or metal/support effects.

4. Conclusions

Gas phase (1 atm, 423 K) continuous hydrodechlorination/hydrogenation of mono- and di-chlorophenols over Pd catalysts is a feasible alternative route to C6ONE. Thermochemical calculations have revealed that hydrodechlorination is not a limiting step for C6ONE production. The following sequence of increasing $Y_{C6ONE,0}$ has been established: PhOH < mono-chlorophenols < di-chlorophenols. We attribute this response to a direct (concerted) conversion of chlorophenols to C6ONE *via* electrophilic hydrogen attack where resonance stabilisation of the positively charged intermediate favours C6ONE formation. Taking 2,4-DCP as a representative feed, C6ONE formation is structure sensitive with higher specific reaction rates over larger Pd particles (3 → 250 nm). The reaction pathway is insensitive to Pd particle size resulting in a common selectivity/conversion profile. Our results demonstrate that the catalytic hydroprocessing of chlorophenols outperforms conventional PhOH hydrogenation to the target C6ONE.

Acknowledgements

The authors acknowledge EPSRC for free access to the TEM facility at the University of St Andrews.

References

1. Mani P (2010) PhD Thesis Title: FTIR, FTR Spectra and Vibrational Analysis of Some Alicyclic and Aromatic Compounds. University of Pondicherry, Pondicherry
2. Vyver SVd, Roman-Leshkov Y (2013) Catal Sci Technol 3 (6):1465-1479
3. Wang Y, Zhang J, Wang X, Antonietti M, Li H (2010) Angew Chem Int Ed 49 (19):3356-3359
4. Romero A, Santos A, Ruiz G, Simón E (2011) Ind Eng Chem Res 50 (14):8498-8504
5. Popova M, Szegedi Á, Lázár K, Dimitrova A (2011) Catal Lett 141 (9):1288-1296
6. Zhong J, Chen J, Chen L (2014) Catal Sci Technol 4 (10):3555-3569
7. Hao J, Cheng H, Wang H, Cai S, Zao F (2007) J Mol Catal A: Chem 271:42-45
8. Xu L-X, He C-H, Zhu M-Q, Fang S (2007) Catal Lett 114:202-205
9. Chen J-R, Chen S-K (2005) J Loss Prev Process Ind 18:97-106
10. Shin E-J, Keane MA (1998) J Catal 173:450-459

11. Mahata N, Raghavan KV, Vishwanathan V, Park C, Keane MA (2001) Phys Chem Chem Phys 3:2712-2719
12. Makino Y (2006) J Alloys Compd 408-412:484-489
13. Claus P, Berndt H, Mohr C, Radnik J, Shin E-J, Keane MA (2000) J Catal 192:88-97
14. Meier H-P, van Esbroeck J, Terweduwe E (1994) Process for Purification of Cyclohexanone. United States Patent 5,292,960, 8 March
15. Arora PK, Bae H (2014) Microb Cell Fact 13:31-49
16. Michałowicz J, Duda W (2007) Polish J of Environ Stud 16 (3):347-362
17. Keane MA (2011) ChemCatChem 3 (5):800-821
18. Dong Z, Dong C, Liu Y, Le X, Jin Z, Ma J (2015) Chem Eng J 270:215-222
19. Molina CB, Pizarro AH, Casas JA, Rodriguez JJ (2014) Appl Catal B: Environ 148–149:330-338
20. Fang D, Li W, Zhao J, Liu S, Ma X, Xu J, Xia C (2014) RSC Adv 4 (103):59204-59210
21. Zhao J, Li W, Fang D (2015) RSC Adv 5 (53):42861-42868
22. Diaz E, Mohedano AF, Casas JA, Calvo L, Gilarranz MA, Rodriguez JJ (2015) Catal Today 241, Part A:86-91
23. Baumgarten E, Fiebes A, Stumpe A (1997) React Funct Polym 33 (1):71-79
24. Roy HM, Wai CM, Yuan T, Kim J-K, Marshall WD (2004) Appl Catal A: Gen 271 (1–2):137-143
25. Newman SG, Jensen KF (2013) Green Chem 15 (6):1456-1472
26. Wiles C, Watts P (2012) Green Chem 14 (1):38-54
27. Ricciardi R, Huskens J, Verboom W (2015) ChemSusChem 8 (16):2586-2605
28. Gutmann B, Cantillo D, Kappe CO (2015) Angew Chem Int Ed 54 (23):6688-6728
29. Baxendale IR (2013) J Chem Technol Biotechnol 88 (4):519-552
30. Gómez-Quero S, Cárdenas-Lizana F, Keane MA (2010) AIchE 56 (3):756-767
31. Cárdenas-Lizana F, Keane MA (2015) Phys Chem Chem Phys 17:28088-28095
32. Hao Y, Wang X, Perret N, Cárdenas-Lizana F, Keane MA (2015) Catal Struct React 1 (1):4-10
33. Cárdenas-Lizana F, Hao Y, Crespo-Quesada M, Yuranov I, Wang X, Keane MA, Kiwi-Minsker L (2013) ACS Catal 3 (6):1386-1396
34. Gómez-Quero S, Cárdenas-Lizana F, Keane MA (2008) Ind Eng Chem Res 47 (18):6841-6853
35. Cárdenas-Lizana F, Pedro ZMd, Gómez-Quero S, Kiwi-Minsker L, Keane MA (2015) J Mol Catal A: Chem 408:138-146
36. Itoh N, Xu W-C (1993) Appl Catal A: Gen 107:83-100
37. Cárdenas-Lizana F, Gómez-Quero S, Perret N, Keane MA (2011) Catal Sci Technol 1:652-661
38. Jongh PEd, Adelhelm P (2010) Nanoparticles and 3D Supported Nanomaterials. In: Hirscher M (ed) Handbook of Hydrogen Storage: New Materials for Future Energy Storage. Wiley, Weiheim, p 294
39. Molina CB, Pizarro AH, Gilarranz MA, Casas JA, Rodriguez JJ (2010) Chemical Engineering Journal 160 (2):578-585
40. Li H, Liu J, Li H (2008) Mater Lett 62:297-300
41. Smith HA, Stump BL (1961) J Am Chem Soc 83:2739-2743
42. Yoneda T, Takido T, Konuma K (2007) J Mol Catal A: Chem 265:80-89
43. Khachatryan L, Lomnickiwo S, Dellinger B (2007) Chemosphere 68 (9):1741-1750

44. Wang R, Chen C-L, Gratzl JS (2005) Bioresour Technol 96 (8):897-906
45. Tang LM, Huang MY, Jiang YY (1996) Chin J Polym Sci 14 (1):57-62
46. Jin Z, Yu C, Wang X, Wan Y, Li D, Lu G (2011) J Hazard Mater 186 (2–3):1726-1732
47. Xia D, Liu L, Huang M-Y, Jiang Y-Y (1999) Polym Advan Technol 10 (1-2):116-119
48. Amorim C, Wang X, Keane MA (2011) Chin J Catal 32 (5):746-755
49. Mahata N, Vishwanathan V (2000) J Catal 196:262-270
50. Chary KVR, Naresh D, Vishwanathan V, Sadakane M, Ueda W (2007) Catal Commun 8:471-477

Table 1: Equilibrium constants (K_j) and fractional conversions (X_i) associated with the consecutive steps in the hydrotreatment of dichlorophenols at 1 atm and 423 K (see dashed arrows in Fig. 1 and eqns. (4-6)).

Reaction step	K_j	X_i
dichlorophenol → PhOH	6×10^{23} atm	1.00
PhOH → C6ONE	1×10^{6} atm^{-2}	1.00
C6ONE → C6OH	47 atm^{-1}	0.86

Table 2: β-Pd hydride decomposition temperature (TPR T_{max} (K)), hydride composition (H/Pd), H_2 chemisorption, Pd particle size (d), surface area (S_{Pd}) and specific initial C6ONE production rate ($(R'_{C6ONE})_0$) for Pd and Pd/Al_2O_3.

Catalyst	Pd	Pd/Al_2O_3-1273	Pd/Al_2O_3
TPR T_{max} (K)	386	371	356
H/Pd	0.69	0.33	0.15
H_2 chemisorption ($\times10^{-2}$ mol mol$_{Pd}^{-1}$)	0.3	8	58
d (nm)	250[a]; 238[b]	13[a]; 10[c]	2[a]; 3[c]
S_{Pd} (m$_{Pd}^2$ g$_{Pd}^{-1}$)[d]	2	38	250
$(R'_{C6ONE})_0$ ($\times10^{-4}$ mol$_{C6ONE}$ h^{-1} m$_{Pd}^{-2}$)	94	68	49

[a]H_2 chemisorption derived Pd particle size
[b]XRD derived Pd particle size
[c]TEM derived Pd particle size
[d]$S_{Pd} = 6/(\rho_{Pd} \times d)$ where ρ_{Pd} = 12.02 g$_{Pd}$ cm$_{Pd}^{-3}$

Table 3: Fractional selectivities ($S_{i,0}$) and C6ONE yields ($Y_{C6ONE,0}$) resulting from the hydrotreatment of PhOH and chlorophenols over Pd; (W/F_{OH}) = 1.33 mol_{Pd} h mol_{OH}^{-1}.

Reactant	$S_{PhOH,0}$	$S_{C6ONE,0}$	$S_{C6OH,0}$	$Y_{C6ONE,0}$
PhOH	-	0.83	0.17	0.62
2-CP	0	0.77	0.23	0.77
3-CP	0	0.76	0.24	0.76
4-CP	0	0.75	0.25	0.75
2,3-DCP	0.07	0.80	0.13	0.80
2,4-DCP[a]	0.10	0.82	0.06	0.82
3,4-DCP[b]	0.19	0.69	0.11	0.69

[a] $S_{2\text{-}CP,0} < 0.02$
[b] $S_{3\text{-}CP,0} < 0.01$

Figure Captions

Fig. 1: Reaction pathways for the production of C6ONE and C6OH through PhOH hydrogenation (dashed box) and chlorophenol(s) hydrodechlorination/hydrogenation (solid box). *Note*: direct and stepwise routes to C6ONE from chlorophenols are identified by bold and dashed arrows, respectively

Fig. 2: (a) TPR profiles and (b) XRD patterns for (I) Pd, (II) Pd/Al_2O_3-1273 and (III) Pd/Al_2O_3. *Note*: JCPDS-ICDD reference data for Pd (05-0681, IV) and γ-Al_2O_3 (10-0425, V) are included in (b)

Fig. 3: Time-on-stream profiles for C6ONE (▲), C6OH (×) and PhOH (◇) production *via* hydrodechlorination/hydrogenation of 2-CP (a,◆), 3-CP (b, ■), 4-CP (c, ★), 2,3-DCP (d, ○), 2,4-DCP (e,△) and 3,4-DCP (f, ●) over Pd: $(W/F_{OH}) = 1.33\ mol_{Pd}\ h\ mol_{OH}^{-1}$. *Note*: lines represent fit to eqn. (7)

Fig. 4: C6ONE yield ($Y_{C6ONE,0}$) resulting from hydrodechlorination/hydrogenation of mono- and di-chlorophenols over Pd: $(W/F_{OH}) = 0.17\ mol_{Pd}\ h\ mol_{OH}^{-1}$

Fig. 5: (a) Representative TEM image with (b) associated particle size distribution for (I) Pd/Al_2O_3-1273 and (II) Pd/Al_2O_3

Fig. 6: (a) C6ONE yield ($Y_{C6ONE,0}$) as a function of contact time (W/F_{OH}) and (b) C6ONE selectivity ($S_{C6ONE,0}$) as a function of 2,4-DCP conversion ($X_{2,4\text{-}DCP,0}$) for hydrodechlorination/hydrogenation over Pd (●), Pd/Al_2O_3-1273 (■) and Pd/Al_2O_3 (▲). *Note*: dashed line in (a) identifies maximum yield under thermodynamic control

Fig. 1

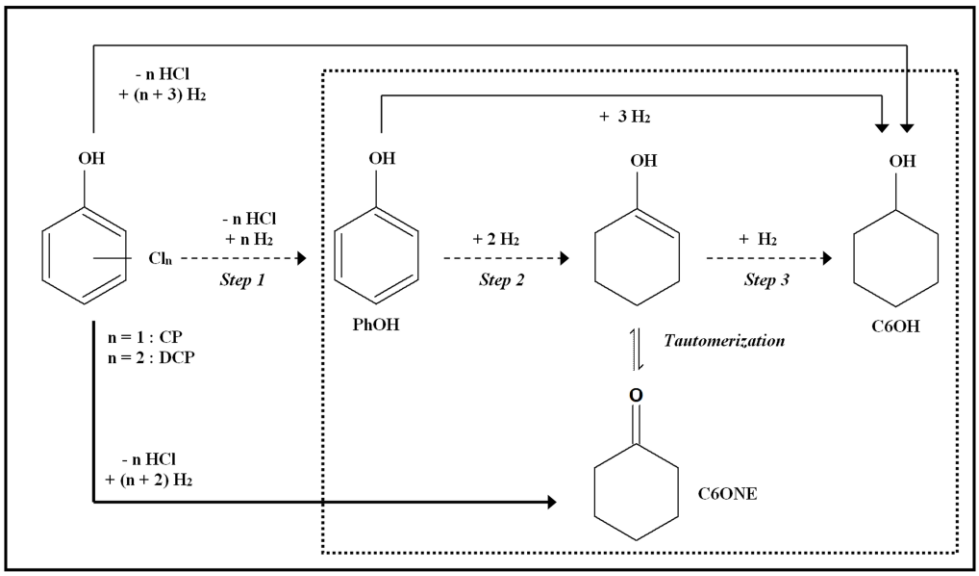
- n HCl
+ (n + 3) H2
+ 3 H2
OH
OH
OH
OH
- n HCl
+ n H2
Cln
Step 1
PhOH
+ 2 H2
Step 2
+ H2
Step 3
C6OH
Tautomerization
n = 1 : CP
n = 2 : DCP
O
- n HCl
+ (n + 2) H2
C6ONE

Fig. 2

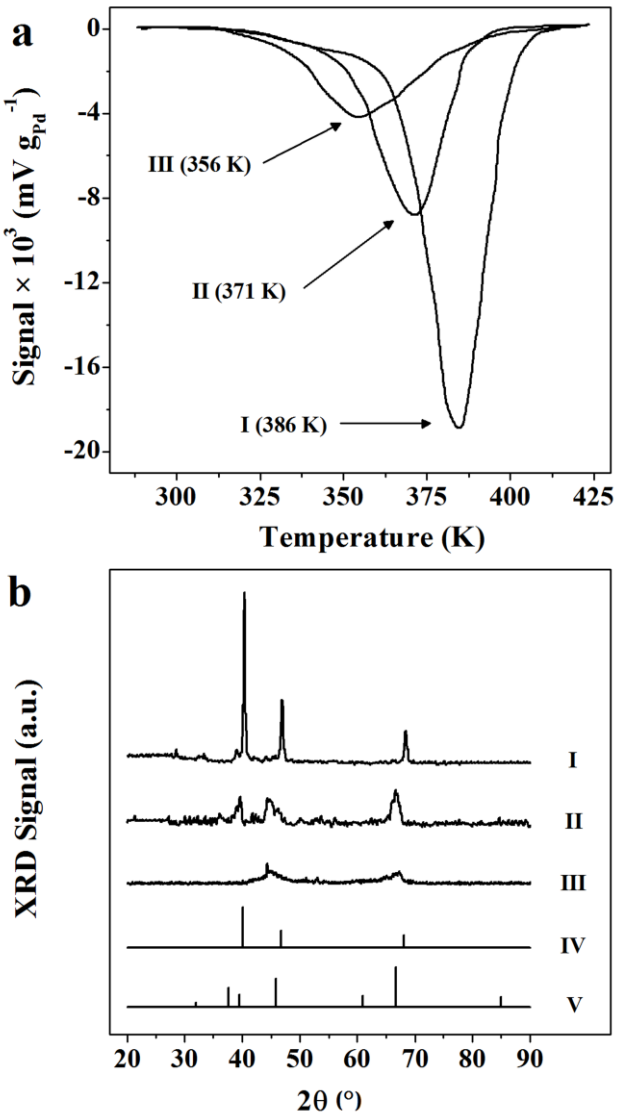
a
Signal × 10^3 (mV g_Pd^-1)
0
-4
-8
-12
-16
-20
III (356 K)
II (371 K)
I (386 K)
300
325
350
375
400
425
Temperature (K)
b
XRD Signal (a.u.)
I
II
III
IV
V
20
30
40
50
60
70
80
90
2θ (°)

Fig. 3

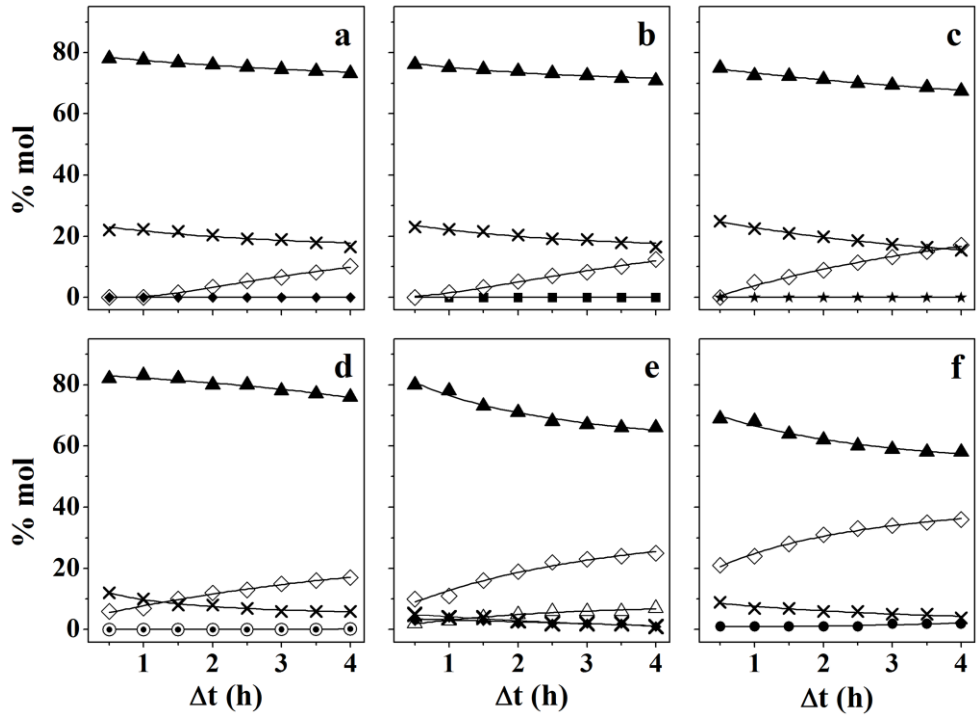

Fig. 4

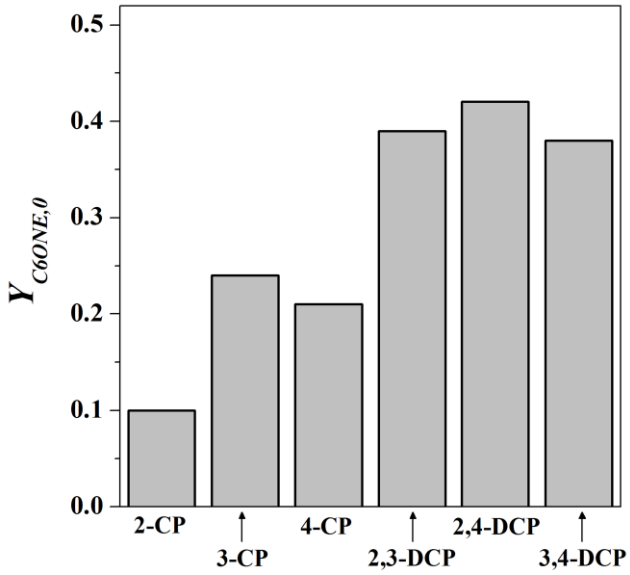

Fig. 5

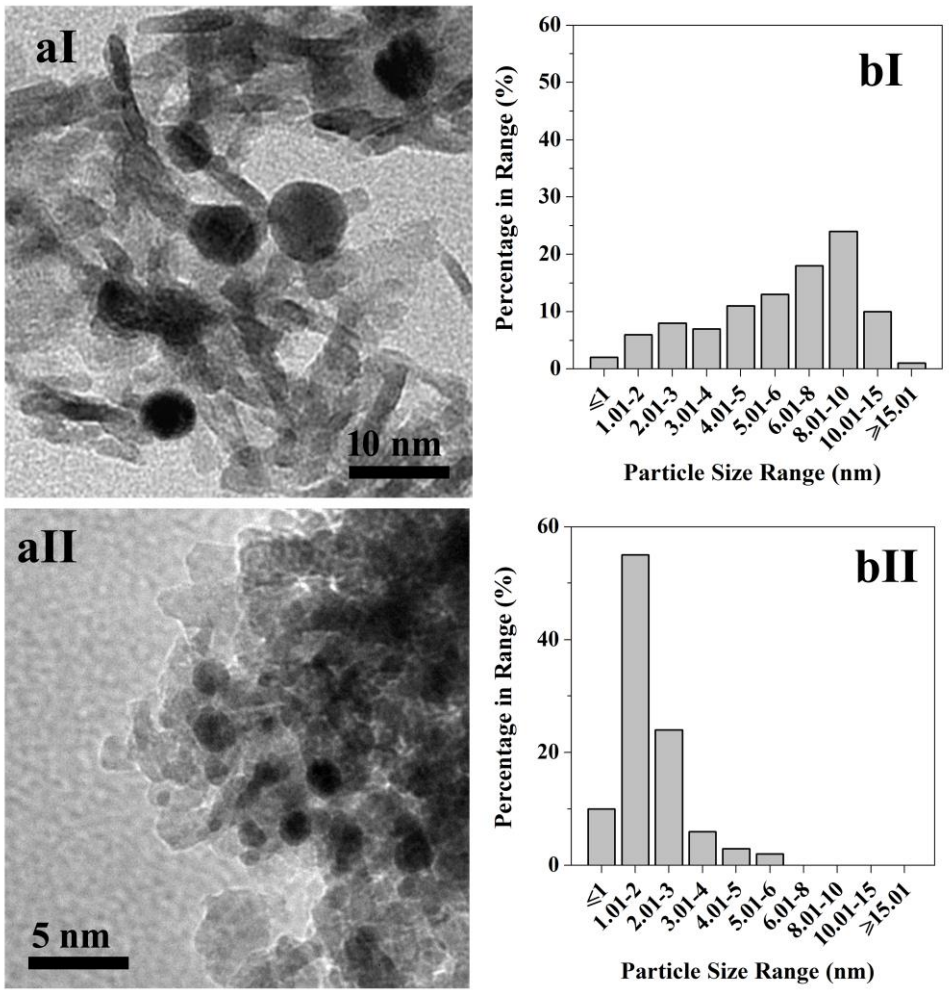
aI
10 nm
bI
Percentage in Range (%)
0
10
20
30
40
50
60
≤1
1.01-2
2.01-3
3.01-4
4.01-5
5.01-6
6.01-8
8.01-10
10.01-15
≥15.01
Particle Size Range (nm)
aII
5 nm
bII
Percentage in Range (%)
0
20
40
60
≤1
1.01-2
2.01-3
3.01-4
4.01-5
5.01-6
6.01-8
8.01-10
10.01-15
≥15.01
Particle Size Range (nm)

Fig. 6

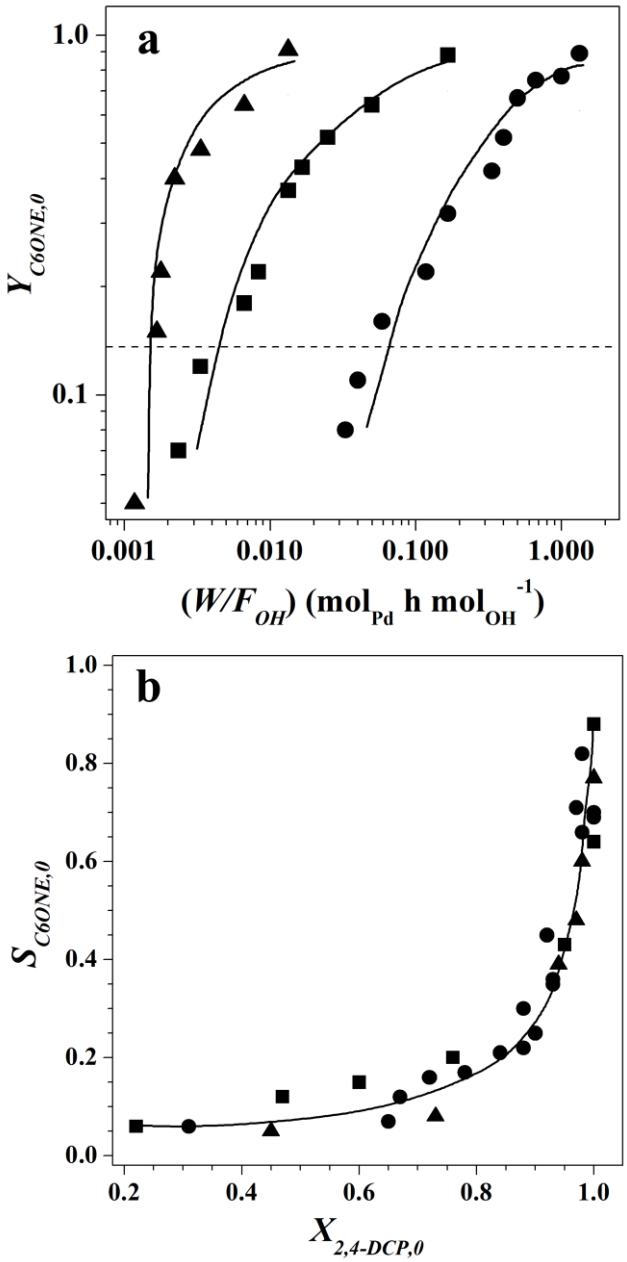
a
1.0
0.1
$Y_{C6ONE,0}$
0.001
0.010
0.100
1.000
(W/F_{OH}) (mol_{Pd} h mol_{OH}^{-1})
b
1.0
0.8
0.6
0.4
0.2
0.0
$S_{C6ONE,0}$
0.2
0.4
0.6
0.8
1.0
$X_{2,4\text{-}DCP,0}$